Design and Performance Study of a Compact SOI Polarization Rotator at 1.55 μm

Ajanta Barh, B. M. Azizur Rahman, *Senior Member, IEEE*, Ravi K. Varshney, and Bishnu P. Pal, *Senior Member, IEEE*

***Abstract*—We numerically design a compact silicon (Si) based polarization rotator (PR) by exploiting power coupling through phase matching between the TM mode of a Si strip waveguide (WG) and TE mode of a Si-air vertical slot WG. In such structures, the coupling occurs due to horizontal structural asymmetries and extremely high modal hybridness due to high refractive index contrast of Si-on-insulator (SOI) structure. Design parameters of the coupler have been optimized to achieve a compact PR of ~ 135 μm length at the telecommunication wavelength of 1.55 μm. Maximum power coupling efficiency (C_m), which is studied by examining the transmittance of light, is achieved as high as 80% for both polarization conversions. Fabrication tolerances and the band width of operation of the designed PR have also been studied.**

***Index Terms*— Polarization sensitive device, Silicon photonics, Si-on-insulator (SOI) waveguides, Slot waveguides.**

I. Introduction

REVOLUTION of the semiconductor electronic technology was only possible due to miniaturization and integration of millions of transistors into a single VLSI chip. Similar to this revolution, the only way to reduce the cost of optoelectronics, which is not limited by electronic speed, is to make the devices as small as possible and find a material system for monolithic integration of all components.

One way of reducing the device size is to use a dielectric material with a refractive index (RI) as high as possible, which can improve the optical confinement and effectively reduce the waveguide dimensions. High index contrast also allows very small bending radius, suitable for increasing number of components on a chip. Silicon (Si) is the most mature material for electronics but relatively a newer material for photonics. However, as the low-cost CMOS facilities can be exploited for the fabrication, Si photonics is becoming a hot research topic today. Silicon-on-insulator (SOI) [1-2] can provide large refractive index contrast between Si core and silica cladding (~ 3). The basic idea is to use the high RI of Si to shrink the optical confinement down to sub-wavelength scale and also to utilize the fabrication infrastructure of CMOS electronics to realize high yield, low cost manufacturing [3-5]. Today, Si-based platforms support the realization of a wide variety of devices, including high-speed modulators and detectors [6], low-loss waveguides [7] and other passive and active [8], linear and non-linear [9] components. Additionally, light from fiber to Si waveguide (WG) can be coupled by especially designed tapers or Bragg gratings. Recently, SOI-based nano sized compact *slot optical* WG has assumed importance due to its potential applications [10]. Due to high index contrast at the interface, electric field normal to the interface shows a very high discontinuity at the interface with very high optical confinement inside the low index slot region when the transverse dimension of the slot is less than the characteristic decay length of that electric field [10-12].

In general, light input to an integrated optical chip is randomly polarized. This polarization of light has a great impact on both photonic circuit design and operation. On the other hand, though the slot and strip WG dimensions are small, they are highly polarization sensitive. Thus, for polarization diversity systems, the problem can be sorted out by incorporating polarization splitter and polarization rotator or converter based on these highly polarization sensitive high RI contrast WGs. The conversion of one polarized mode to the orthogonal polarized mode can be realized by efficient power coupling between these two modes at the *phase matching* or *resonance* condition.

Recently, polarization rotator (PR) made of horizontal slot and strip WG has been reported based on mode evolution [13]. Its fabrication poses difficulty as required proper control of tapered structure is relatively difficult to realize. Moreover, it can rotate only one polarization state for one input direction. Three WGs-based polarization splitter and rotator have been reported [14-15]. Another approach is made for this TE-TM conversion based on 2-D photonic crystal slab WG [16]. In this case though the conversion is good, the structure itself is complicated. Researchers have also tried to implement TE to TM convertor by increasing the polarization crosstalk in μ-bend Si WG [17]. Here also the conversion efficiency is very high though very sensitive to issues like bend loss, bend angle, smooth wall of the WG around bent region etc.

In this paper, we propose a design for realizing a PR for potential application at the optical communication wavelength of 1.55 μm that should be relatively easy to fabricate as no tapering is required and the whole structure, made of two WGs

Partial funding by UKIERI is gratefully acknowledged.

Authors Ajanta Barh, Ravi K. Varshney, and Bishnu P. Pal are with the Department of Physics, Indian Institute of Technology Delhi, Hauz Khas, New Delhi 110016 India (e-mail: ajanta.barh@gmail.com, varshney_rk_iitd@yahoo.com, and bppal@physics.iitd.ernet.in, respectively).

B. M. Azizur Rahman is with the School of Engineering and Mathematical Sciences, City University London, London EC1V 0HB UK (e-mail: b.m.a.rahman@city.ac.uk).

(one is a strip and other one is a vertical slot WG), can be made with a single mask. Moreover, it can rotate both polarization states for a single input direction (i.e., at the coupling length (L_c), TM input in the Si strip WG would yield TE output from the slot WG and TE input in the slot WG would yield TM output from the strip WG). Similar concepts have recently been reported [18-19] to design TE-TM based polarization splitter/rotator, but detailed analysis of various WG parameters, the effects of unwanted mode coupling and their propagation analysis were missing in them. In our simulations, we have analyzed all the aforementioned parameters in details along with the tolerance study. Additionally, our design is optimized both for TE to TM conversion and vice versa. In the present configuration, we have shown that it is possible to match and couple two different polarization states by exploiting efficient coupling between a Si strip WG and an air-Si vertical slot WG. Maximum power coupling efficiency (C_m) ~ 80% is possible for a device length of 134.5 μm. Device performance is studied on the basis of fabrication tolerances and operating band width (BW).

II. Theory

When designing a PR, accurate calculation of the mode effective indices and modal fields corresponding to dominating and non-dominating field components for TE-like and TM-like modes are very important. For high RI contrast WGs, where the modal hybridness and coupling is very strong, the full-vectorial mode solver is essential. For our design a full vectorial finite element method (FV-FEM) was implemented to analyze the 2-D structure. All the vector fields are investigated and depending on modal hybridness, TE and TM modes are identified. In the design process, it is necessary not only to increase the magnitude of the non-dominant field components but its profile can be optimized to enhance its overlap with the dominant field components to achieve the maximum polarization coupling. As all the H-field components are continuous across the dielectric interface, H-field based FV-FEM is used for modal analysis. Based on this FV-FEM the polarization beat length between the TE-like and TM-like fundamental modes is calculated.

Study of propagation of these two orthogonal modes is carried out by "Eigenmode Expansion" method using the commercially available FIMMPROP software. Eigenmode Expansion is a rigorous technique to simulate electromagnetic propagation, which relies on the decomposition of the electromagnetic fields into a basis set of local eigenmodes (including all guided and radiation modes) that exist at the junction of a discontinuity plane. The coefficients of the eigenmodes were calculated by enforcing the continuity of the tangential components of electric and magnetic-fields at the boundaries/junctions. This is fully bi-directional and vectorial algorithm, making no approximations about the polarization state of light, and is a rigorous solution to Maxwell's Equations [20-21]. Here we have launched TE-like and TM-like mode as the input at respective WGs and studied the power propagation along its length.

III. Results and Discussions

A. Proposed Design

Our proposed PR is a coupler based on one Si-strip WG and one Si-air vertical slot WG. The cross-section is shown in Fig. 1. Here two WG's are implemented on silica (SiO_2) as the substrate with air as cover and slot material. However, we can use any low index compatible materials for the slot region, such as electro-optic materials for high-speed modulators [6], doped material to achieve gain [8] or sensing material for efficient organic/inorganic sensing [22]. Vertical slot WG will only support a TE mode (E_x is the dominant component) with higher field inside the slot region. So, here confinement of the fundamental TE mode in slot WG and TM mode in strip WG is considered. Note that, introduction of low index region in slot WG reduces its effective index of fundamental TE mode (n_{eff} –TE) with respect to n_{eff} –TE of strip WG. However this n_{eff} –TE of slot WG becomes more comparable to effective index of the fundamental TM mode (n_{eff} –TM) in strip WG. Thus by proper tuning of WGs parameters, efficient power coupling between these two modes is possible exploiting their extremely high modal hybridness.

We have taken the same height for both the WGs as H and same width for the high index regions of the slot WG as W_2. The width of the strip WG core and low index region of slot WG are taken as W_1 and W_s, respectively. The separation between two WGs is denoted as S (see Fig. 1). Material dispersion of Si and SiO_2 are incorporated through Sellmeier formula. Our working wavelength is 1.55 μm, for which the refractive indices of Si and SiO_2 are 3.47548 and 1.44402, respectively.

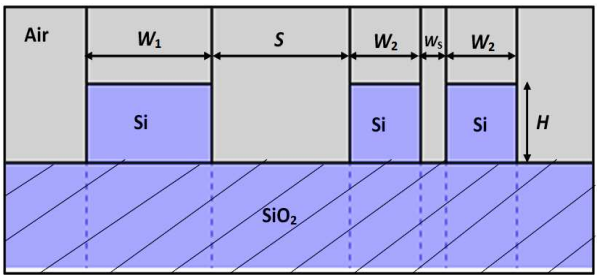

Fig. 1. Schematic transverse view of the proposed polarization rotator.

B. Optimum Structure Parameter

For moderate electric field confinement in the slot, we choose W_s as 90 nm. Fabrication simplicity requires same height (H) for both WGs. Now for sufficient confinement of TM mode inside the strip WG at 1.55 μm wavelength, H should be > 200 nm. In this design work, H is fixed at 220 nm, which is the thickness of most commonly available Si wafer. On the other hand, maintaining TE as the fundamental mode in slot WG, W_2 was chosen to be 255 nm for H = 220 nm. Thus the optimized parameters for the slot WG were W_2 = 255 nm, W_s = 90 nm, H = 220 nm. In the absence of strip WG, the n_{eff} of the TE mode in this slot WG is 1.53716.

Then we have studied n_{eff} for the TM mode of an isolated strip WG of same height by varying its width (W_1). For W_1 = 451 nm, the strip WG's TM mode's n_{eff} becomes equal to n_{eff}

of the TE mode of the slot WG (shown in Fig. 2). Fig. 2 reveals that as we increase W_1, its n_{eff} –TM increases and at the crossing point TM mode for W_1 = 451 nm has the same effective index (n_{eff}) as that of the TE mode for the fixed W_2 and W_s. Then for the combined coupled structure, using these optimized dimensions (i.e. W_1 = 451 nm, W_2 = 255 nm, W_s = 90 nm, H = 220 nm), the variation of n_{eff} of the two orthogonal polarized supermode states were studied as a function of S to determine the mode exchange regime.

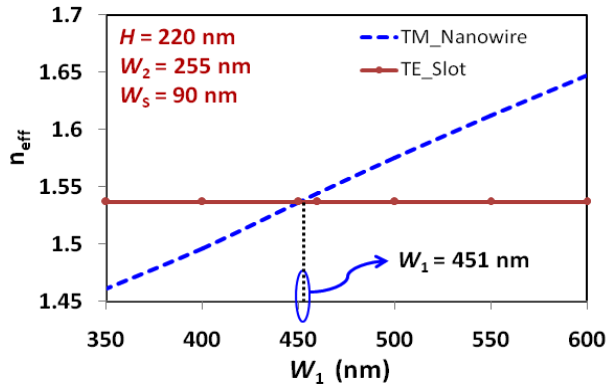

Fig. 2. Variation of n_{eff} –TM of strip WG with W_1 in the absence of slot WG. The horizontal line represents the n_{eff} -TE (1.53716) inside the Slot WG in absence of strip WG.

The three basic parameters to study the supermodes in a PR are n_{eff}, hybridness and coupling length (L_c). For three different S values (450 nm, 500 nm, 550 nm), the variation of above mentioned parameters were studied as a function of strip WG width (W_1) and the corresponding variations are shown in Figs. 3-5, respectively. In Fig. 3, horizontal line represents n_{eff} -TE in the slot (almost constant). Slanted line represents n_{eff} -TM in strip WG, changing as W_1 is increased. But, they do not cross (similar as any coupled structure), but around this region both the polarized supermodes go through a transformation. Near the phase matching condition, two effective indices are close to each other and the phase difference between these modes $\Delta\beta$ will be smaller. For larger S, these n_{eff} curves come closer due to weaker interactions and the minimum $\Delta\beta$ will be smaller.

Around anti-crossing point, these two modes become degenerate and they get mixed up. For a quasi-TE mode, the H_y component is dominant whereas for a quasi-TM mode, its H_x component is dominant. Near anti-crossing the non-dominant field starts increasing leading to higher modal hybridness, which can be defined as the ratio of the maximum values of the H_y to H_x field components for the TM and similarly H_x/H_y for the TE mode. In Fig. 4, at lower W_1, the mode is near quasi-TM, with H_y component being much smaller. So its hybridness is low. As W_1 increases, it travels through the anti-crossing region leading to stronger mode mixing and higher hybridness. At a higher W_1, away from this anti-crossing region, again hybridness reduces. All the peaks appear around the mode exchange regime with increasing value as S decreases. Note that for smaller S, curves are wider as interaction become easier. Similar results can be obtained for TE mode also, but not shown here.

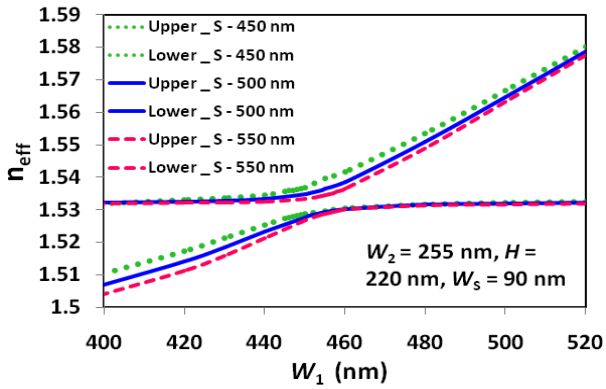

Fig. 3. Upper & lower n_{eff} variation with strip WG width (W_1) for three different S = 450 nm, 500 nm, 550 nm.

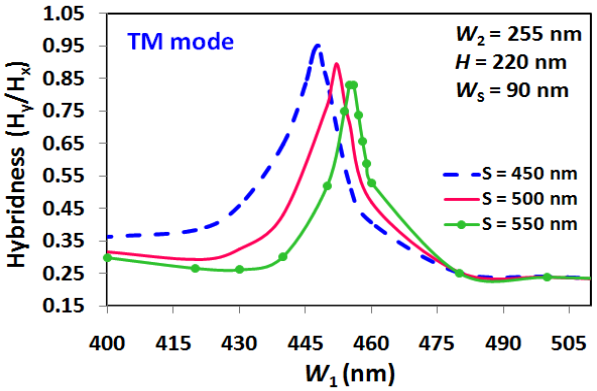

Fig. 4. Variation of modal hybridness of the TM mode with W_1 for three different values of S = 450 nm, 500 nm, 550 nm.

Polarization coupling length of the two modes are defined as ($L_c = \pi / |\beta_1 - \beta_2|$) where, β_1 and β_2 are the propagation constants of the TE and TM modes. From Fig. 5 we can infer that, as S increases, coupling become weaker, and hence, ($\beta_1 - \beta_2$) is getting smaller near anti-crossing point, so peak L_c become larger. From Figs. 4 and 5, it should be noted that as S is reduced the phase matching value of W_1 reduces. When a directional coupler is composed of two identical WGs, they are always phase matched or synchronous. But, for a synchronous coupler composed of non-identical waveguides, its phase matching also depends on mutual loading of the waveguides. Consequently, the phase matching condition for W_1 value changes with S, as shown here.

The maximum L_c and variation in maximum power coupling efficiency (C_m) with W_1 is shown in Table I. Where C_m is the maximum normalized power coupled from one polarized mode to the other polarized mode. From this table, we can infer that the L_c decreases with the decrement of separation between the two WGs. Additionally, due to stronger coupling between the two WGs, the supermodes deviate from just being formed out of linear combinations of isolated modes (as in weak coupling case) and as a result progressively less power will be transferred from one WG to

another and hence C_m also deceases. Thus there exists a trade-off between these two parameters. Here we can see that to achieve ~ 80% power conversion, the minimum separation (S) would be ≈ 500 nm for which the L_c becomes ≈ 134.5 μm. We have therefore focused our further study for S = 500 nm.

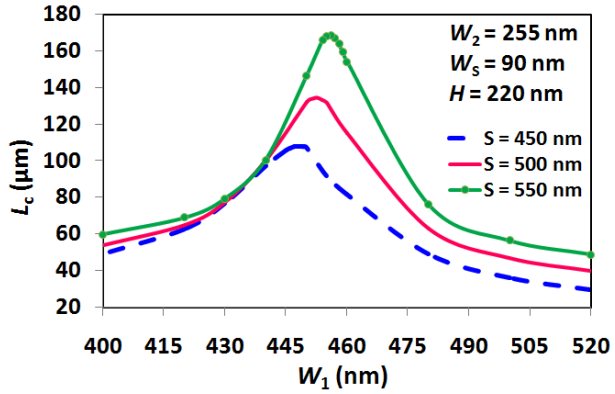

Fig. 5. Variation of coupling length (L_c) with W_1 for three different S = 450 nm, 500 nm, 550 nm.

TABLE I
PHASE MATCHING W_1, L_c AND C_m FOR DIFFERENT S AT 1.55 μm

S (nm)	W_1 (nm)	L_c (μm)	C_m (%)
600	454.5	211.51	87.04
550	453	168.45	82.20
500	451	134.50	79.01
450	447	108.01	73.64
400	442	87.16	66.02

C. *Supermodes of PR*

For further analysis, we have fixed the structure parameters as W_1 = 451 nm, W_2 = 255 nm, W_s = 90 nm, H = 220 nm, S = 500 nm. The supermodes of this designed PR are shown in Figs. 6–8, where the z-component of Poynting vector (P_z), H_y and H_x fields of dominating TM mode in strip WG are displayed, respectively.

The transverse distribution of the P_z (x,y) is shown in Fig. 6, which shows evenly distributed powers in the two WGs. Although maximum amplitudes in two constituent waveguides are different as their core-sizes were also different, confinement factors in each WG were also calculated. The confinement factors in the two WGs for both the supermodes were similar when the two polarized modes were phase matched. However, the supermodes were neither quasi-TE nor quasi-TM, but polarized differently in two constituents WGs with its H_y and H_x components nearly equal (see Fig. 4). Additionally, their shapes in the two WGs are different as the waveguides were of different shapes, although phase matched. However, as this is the phase matched structure, the two constituent waveguides carry nearly equal amounts of power. In order to illustrate it, we have plotted H_y and H_x fields of the supermode in Figs. 7 and 8, respectively.

Fig. 7 clearly indicates that H_y is in the slot region, which supported the interacting TE mode. Note the two peaks of H_y field in the slot guide, which is typical for a slot WG [10]. There is a small amount of H_y in the strip WG. This is an indication of very high hybridness of the supermode.

Fig. 8 shows the H_x field of the supermode, which is the dominating TM mode in strip WG. It is mainly confined in the strip WG and a small amount of H_x field lie in the slot WG. It can be clearly seen that both the signs of H_y in Fig. 7 and H_x in Fig. 8 are positive. Thus it is the even supermode of the whole structure. For the sake of brevity, the other supermode is not shown here, whose H_x and H_y field components were of different signs, similar to the field profile of an odd supermode.

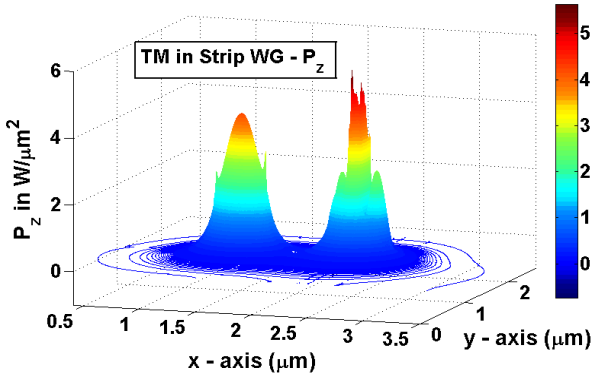

Fig. 6. Amplitude plot of P_z (x,y) of dominating TM mode in strip WG.

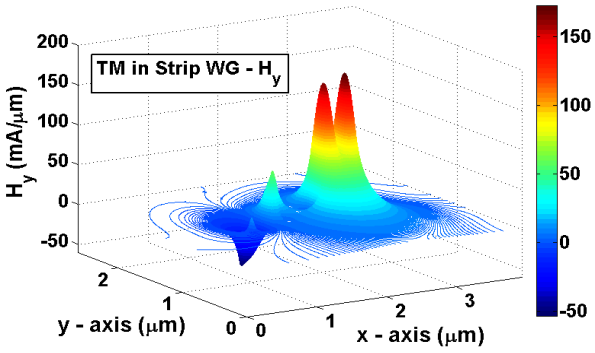

Fig. 7. Amplitude plot of H_y (x,y) of dominating TM mode in strip WG.

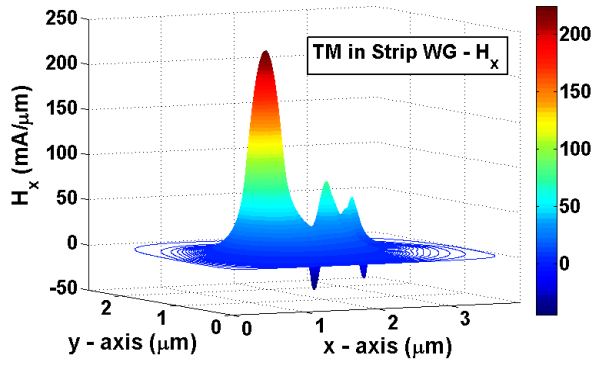

Fig. 8. Amplitude plot of H_x (x,y) of dominating TM mode in strip WG.

D. Mode Propagation in PR

Propagation of TE and TM modes along the device is studied by launching the TE-like mode in slot WG and TM-like mode in strip WG. By assuming TE-like input in slot WG, the intensity variation of TE mode in slot WG and TM mode in strip WG are shown in Fig. 9. It can be clearly seen that, the maximum power of input TE mode transfers to TM mode at device length of 134.5 µm, which is nothing but the L_c of these two modes (see Table I). It can be appreciated more prominently from Fig. 10, where the variations of normalized power (P_N) along propagation length is shown for these two modes. The power is calculated by integrating H_y/E_x fields (for TE mode) and H_x/E_y fields (for TM mode) around each WG area. Maximum P_N for the output TM mode is ~ 80%. Note that, we had normalized the input power to 1, however, as this mode is highly hybrid in nature, only 93% power is due to the H_y or E_x (TE-Slot). Thus with respect to input power in TE mode (H_y or E_x), the maximum output power coupling efficiency to TM mode (H_x or E_y) is ~ 86% at optimized device length of 134.5 µm. A small ripple in Fig. 10 can also be noticed with a beat length of ~ 13 µm, which is due to periodic mode coupling to TM-like mode of the slot WG. Additionally, the difference between n_{eff} values of TE-slot and TE-strip is quite large ($\Delta n_{eff} > 0.7$), thus coupling to TE-strip is inefficient, and not visible in Fig. 10.

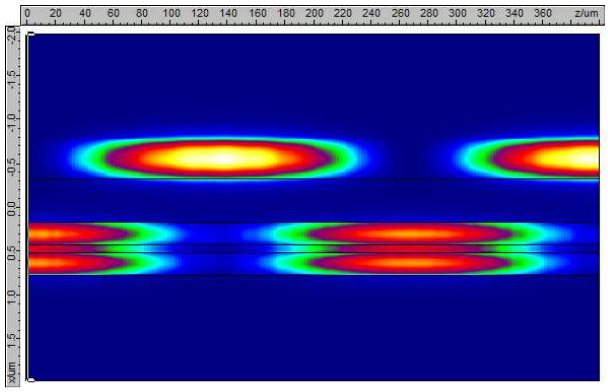

Fig. 9. Intensity (time average) variations along device length of TE mode in the slot WG and TM mode in the strip WG for TE-like input in the slot WG.

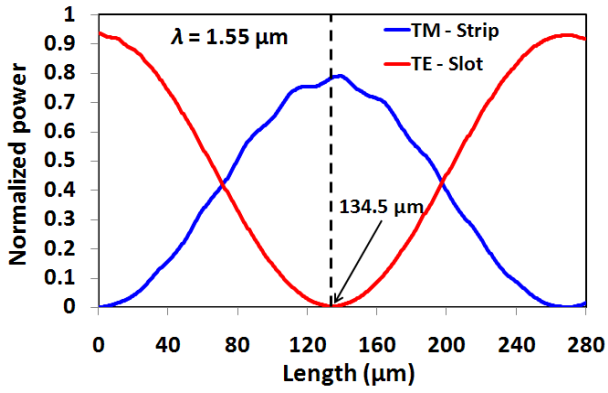

Fig. 10. Normalized Power variations along the device length of TE mode in the slot WG (Red curve) and TM mode in the strip WG (Blue curve).

This ripple phenomenon is more prominent for TM-like input in Si strip WG. For this case, the intensity variations of TE mode in slot WG and TM mode in strip WG are shown in Fig. 11. Also from this figure, it is evident that, the total power of input TM mode transfers to TE mode at a device length of ~ 135 µm. Variation of P_N along the propagation length is shown in Fig. 12, where power variation in all four modes (fundamental TE & TM mode in slot WG and strip WG) is displayed. Here input TM mode (Green curve) in strip WG couples not only to TE mode of slot (Red curve) WG but also to TM mode of slot WG (Blue curve). The index difference between these two TM modes is quite small (~ 0.05) which results in significant power exchange (beat length is ~ 13 µm, which agrees with the corresponding $\Delta\beta$ of these two modes) between them and hence the oscillation in the blue and green curves. However, the important thing is, their sum gives total TM power which is decreasing along the propagation distance as TE power builds up in slot WG and at the designed device length (L = 134.5 µm), P_N is maximum in the TE mode at the output of slot WG, with C_m > 80%.

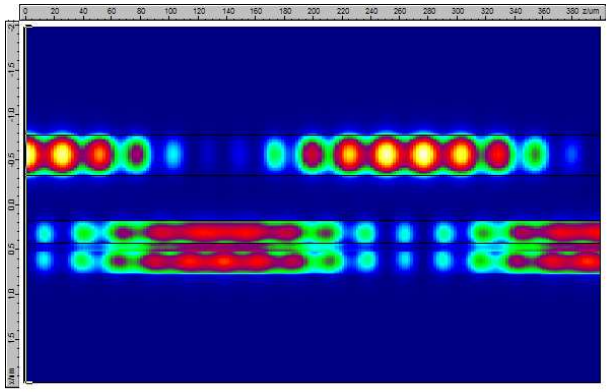

Fig. 11. Intensity (time average) variations along device length of TE mode in the slot WG and TM mode in the strip WG for TM-like input in strip WG.

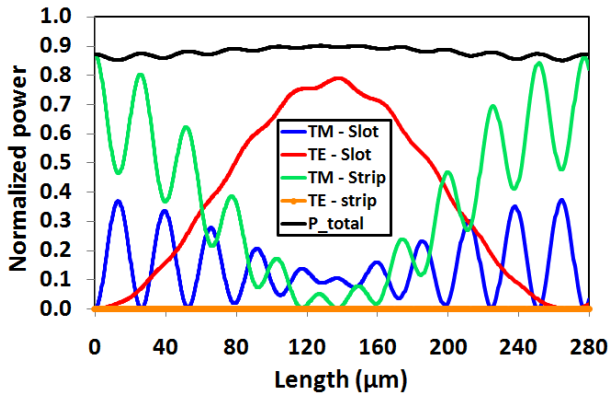

Fig. 12. Normalized Power variations along device length of TE mode in slot (Red curve), TM mode in strip (Green curve), TM mode in slot (Blue curve), TE mode in strip (Orange curve) WGs and total guided power (Black curve).

The total output power (P_total), which is the physical sum of powers carried by four modes of the two isolated WGs, is shown by a solid black line in Fig. 12. It indicates that about 10% of the total input power would have probably lost in the form of radiation modes and also a small amount as reflected

power at junction. However, the total power with propagation approximately remains constant. All four powers are calculated around the slot/strip WG core region but not across the entire cross section of the coupled structure. Thus, the small fraction of power, associates with the evanescent fields present has been effectively neglected, which might have caused the small ripple seen in the P_total. On the other hand, in the FIMMPROP software, instead of exact modal powers, the TE and TM mode powers were calculated from their dominating E_x/H_y and E_y/H_x components, respectively. However, since the quasi-TE and TM modes were hybrid having all the four transverse components of the E and H fields, this may lead to small ripple.

E. Tolerance Study of Designed PR

From potential fabrication point of view, we have also studied the tolerance of the structure by varying some of the WG parameters like, W_1 by ± 6 nm and W_s by ± 4 nm and shown the corresponding variations in Figs. 13-14, respectively. In general, waveguide fabricated by using the CMOS technology, the fabrication tolerance of its height is significantly better, so only the effect of variation in its width is studied here. The variation of the polarization conversion with the fabrication tolerances of W_1 and W_s are shown in Figs. 13-14, respectively. For both the cases, C_m drops from its maximum value with the shift in optimum structure parameters. For a change of ± 6 nm of the strip width, the power conversion is 1.2 dB lower. Power conversion with change in slot width is more sensitive. For a change of ± 2 nm of the slot width, the power conversion drops by ~ 1 dB. However, it may be possible to correct fabrication tolerances by post-trimming of the WGs or through temperature (T) tuning. By changing T, the RI of Si and SiO_2 can be changed [23-24]. As a result, n_{eff} of individual guides undergoes unequal change.

We have calculated the phase matching WG parameters by increasing T by 10 K. For fixed slot WG structure (W_2 = 255 nm, W_s = 90 nm, H = 220 nm), phase matched strip width (W_1) becomes ~ 448 nm for fixed H (220 nm). On the other hand, for fixed strip WG structure (W_1 = 451 nm, H = 220 nm), phase matched slot width (W_s) becomes ~ 88 nm for fixed W_2 = 255 nm and H = 220 nm. Thus by tuning T, phase matching condition can be tuned appropriately.

F. Band Width of Operation

We have also studied the band width of operation for the designed PR by studying the variation of C_m with operating wavelength (λ). This variation is shown in Fig. 15. The figure shows that the designed devices are reasonably robust with respect to change in λ falling within the so-called C-band of an EDFA amplifier.

Note that, for Figs. 13-15, C_m is shown for two sets. One is for proposed device length (L = 134.5μm) and other is for the maximum possible power conversion of the modified structure, at L_c. This L_c is different from L as for each change in WG dimension ($\pm\Delta W_1$ or $\pm\Delta W_s$ or $\pm\Delta\lambda$), phase matching condition also changes.

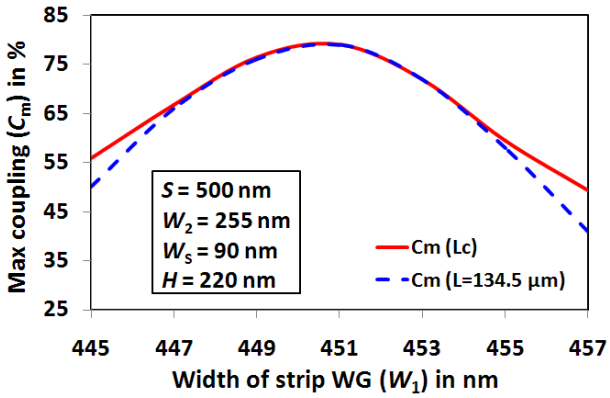

Fig. 13. Tolerance study for C_m with variation in W_1. Red solid curve corresponds to C_m at L_c for different W_1. Blue dashed curve corresponds to C_m at device length.

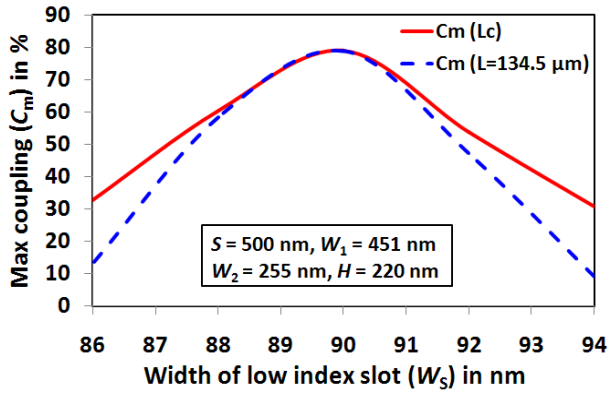

Fig. 14. Tolerance study for C_m with variation in W_s. Red solid curve corresponds to C_m at L_c for different W_s. Blue dashed curve corresponds to C_m at device length.

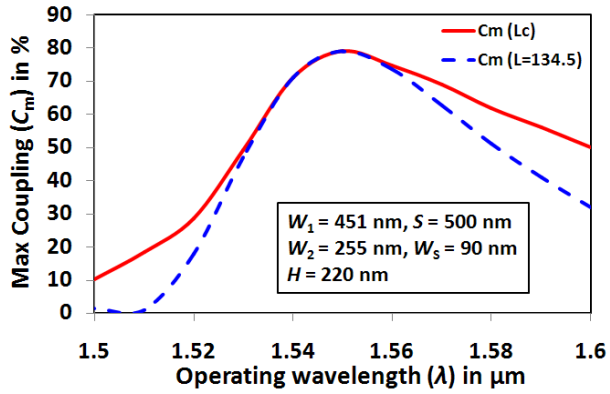

Fig. 15. Variations of C_m with operating wavelengths. The red solid curve corresponds to C_m at L_c for different wavelength and blue dashed curve corresponds to C_m at device length.

IV. CONCLUSION

Through a detailed numerical study, a novel design of a compact SOI polarization rotator incorporating optical coupling between one Si-strip WG and one Si-air vertical slot WG is presented. The above results suggests that an appreciable short 134.5 μm long PR can be designed for 1.55 μm wavelength by exploiting the phase matching between the orthogonally polarized modes of these two guides. Maximum

power coupling efficiency of 80% is possible from input TE to output TM mode and vice versa. Fabrication tolerances of the designed structure were studied by varying different WG parameters and we have suggested that, this may be corrected through appropriate temperature tuning. Our "band width of operation" reveals that the device is reasonably robust with respect to the change in operating wavelength. This design should be relatively easy to implement for fabrication and can be made with a single mask. Moreover, it can rotate both the polarization states for a single input direction. Thus, this high conversion efficiency, low footprint, simpler design, along with the existence of well-matured fabrication technologies [2,5,7] for SOI structures, should make our proposal attractive for making an on-chip polarization rotator for potential deployment at the optical communication wavelength of 1.55 μm.

ACKNOWLEDGMENT

Author A.B. gratefully acknowledges the support of CSIR, India for her Ph.D. fellowship. This work was originally conceived under the UKIERI Indo-British collaboration project (2007-2011) on Application-specific Microstructured Optical Fibers when A.B. made an academic exchange visit to City University London. We thank Kamal Kishor for providing us the trial version of FIMMPROP, Photon Design (UK) software©.

REFERENCES

[1] W. Bogaerts, D. Taillaert, B. Luyssaert, P. Dumon, J. Van Campenhout, P. Bienstman, D. Van Thourhout, R. Baets, V. Wiaux, and S. Beckx. (2004, Apr.). Basic structures for photonic integrated circuits in silicon-on-insulator. *Opt. Express.* [Online]. *12 (8)*, pp. 1583-1591. Available: http://www.opticsinfobase.org/oe/abstract.cfm?uri=oe-12-8-1583

[2] W. Bogaerts, R. Baets, P. Dumon, V. Wiaux, S. Beckx, D. Taillaert, B. Luysseart, J. Van Campenhout, P. Bienstman, and D. Van Thourhout. (2005, Jan.). Nanophotonic waveguides in silicon-on-insulator fabricated with CMOS technology. *J. Lightwave Technol.* [Online]. *23 (1)*, pp. 401–412. Available: http://ieeexplore.ieee.org/xpls/abs_all.jsp?arnumber=1377470&tag=1

[3] L. Tsybeskov, D. Lockwood, and M. Ichikawa, "Silicon photonics: CMOS going optical," in *Proc. of the IEEE*, 2009, pp. 1161-1165.

[4] B. P. Pal, "Guided-wave optics on silicon: Physics, technology, and status," in *Progress in Optics*, vol. 32, 1993, pp. 1-59.

[5] G. T. Reed, "Silicon photonics: The state of the art," John Wiley & Sons Ltd., Chichester, 2008.

[6] T. B. Jones, M. Hochberg, G. Wang, R. Lawson, Y. Liao, P. A. Sullivan, L. Dalton, A. K. Y. Jen, and A. Scherer. (2005, Jul.). Optical modulation and detection in slotted silicon waveguides. *Opt. Express*. [Online]. *13 (14)*, pp. 5216-5226. Available: http://www.opticsinfobase.org/oe/abstract.cfm?uri=oe-13-14-5216

[7] J. Cardenas, C. B. Poitras, J. T. Robinson, K. Preston, L. Chen, and M. Lipson. (2009, Mar.). Low loss etch less silicon photonic waveguides. *Opt. Express*. [Online]. *17 (6)*, pp. 4752 – 4757. Available: http://www.opticsinfobase.org/oe/abstract.cfm?uri=oe-17-6-4752

[8] P. Pintus, S. Faralli, and F. Di Pasquale. (2010, Oct.). Low-threshold pump power and high integration in Al_2O_3: Er^{3+} slot waveguide lasers on SOI. *IEEE Photonics Technology Lett.* [Online]. *22 (19)*, pp. 1428-1430. Available: http://ieeexplore.ieee.org/stamp/stamp.jsp?arnumber=05492163

[9] R. M. Osgood, Jr., N. C. Panoiu, J. I. Dadap, X. Liu, X. Chen, I-Wei Hsieh, E. Dulkeith, W. M. Green, and Y. A. Vlasov. (2009, Jan.). Engineering nonlinearities in nanoscale optical systems: Physics and applications in dispersion-engineered silicon nanophotonic wires. *Advances in Optics and Photonics.* [Online]. *1 (1)*, pp. 162–235. Available: http://www.opticsinfobase.org/aop/abstract.cfm?uri=aop-1-1-162

[10] V. R. Almeida, Q. Xu, C. A. Barrios, and M. Lipson. (2004, Jun.). Guiding and confining light in void nanostructure. *Opt. Lett.* [Online]. *29 (11)*, pp. 1209-1211. Available: http://www.opticsinfobase.org/ol/abstract.cfm?uri=ol-29-11-1209

[11] Q. Xu, V. R. Almeida, R. R. Panepucci, and M. Lipson. (2004, Jul.). Experimental demonstration of guiding and confining light in nanometer-size low-refractive-index material. *Opt. Lett.* [Online]. *29 (14)*, pp. 1626-1628. Available: http://www.opticsinfobase.org/ol/abstract.cfm?uri=ol-29-14-1626

[12] N. N. Feng, J. Michel, and L. C. Kimerling. (2006, Sept.). Optical field concentration in low index waveguides. *IEEE Journal of Quantum Electronics*. [Online]. *42 (9)*, pp. 885–890. Available: http://ieeexplore.ieee.org/xpls/abs_all.jsp?arnumber=1661786

[13] N. N. Feng, R. Sun, J. Michel, and L. C. Kimerling. (2007, Aug.). Low-loss compact-size slotted waveguide polarization rotator and transformer. *Opt. Lett*. [Online]. *32 (15)*, pp. 2131-2133. Available: http://www.opticsinfobase.org/ol/abstract.cfm?uri=ol-32-15-2131

[14] M. Komatsu, K. Saitoh, and M. Koshiba. (2009, Oct.). Design of miniaturized silicon wire and slot waveguide polarization splitter based on a resonant tunneling. *Opt. Express*. [Online]. *17 (21)*, pp. 19225–19234. Available: http://www.opticsinfobase.org/oe/abstract.cfm?uri=oe-17-21-19225

[15] D. M. H. Leung, B. M. A. Rahman, and K. T. V. Grattan. (2011, Jun.). Numerical analysis of asymmetric silicon nanowire waveguide as compact polarization rotator. *IEEE Photonics Journal*. [Online]. *3 (3)*, pp. 381-389. Available: http://ieeexplore.ieee.org/xpls/abs_all.jsp?arnumber=5744087

[16] X. Zhi-Gang, L. Zhi-Yuan, and Z. Dao-Zhong. (2008, Mar.). TM-like and TE-like modes coupling in a two dimensional photonic crystal slab composed of truncated cone silicon rods. *Chin. Phys. Lett.* [Online]. *25 (6)*, pp. 2089-2092. Available: http://cpl.iphy.ac.cn/EN/abstract/abstract35676.shtml

[17] T. Baba, "Si photonic wire waveguides," in *Proc. of SPIE*, 2004, pp. 150-157.

[18] B. Wohlfeil, L. Zimmermann, and K. Petermann. (2012, Jun.).Asymmetric codirectional coupler between regular nanowaveguide and slot-waveguide for polarization conversion. Presented at Advanced Photonics Congress. [Online]. Available: http://www.opticsinfobase.org/abstract.cfm?URI=IPRSN-2012-ITu2B.5

[19] Y. Fei, L. Zhang, T. Cao, Y. Cao, and S. Chen. (2012, Dec.). Ultracompact polarization splitter-rotator based on an asymmetric directional coupler. *App. Opt.* [Online]. *51 (34)*, pp. 8257-8261. Available: http://www.opticsinfobase.org/ao/abstract.cfm?uri=ao-51-34-8257

[20] B. M. A. Rahman and J. B. Davies. (1988, Jan.). Analysis of optical waveguide discontinuities. *J. Lightwave Technol.* [Online]. *6 (1)*, pp. 52–57. Available: http://ieeexplore.ieee.org/xpls/abs_all.jsp?arnumber=3963

[21] G. V. Eleftheriades, A. S. Omar, L. P. B. Katehi, and G. M. Rebeiz. (1994, Oct.). Some important properties of waveguide junction generalized scattering matrices in the context of the mode matching technique. *IEEE Trans. on Microwave Theory and Techniques*. [Online]. *42 (10)*, pp. 1896-1903. Available: http://ieeexplore.ieee.org/stamp/stamp.jsp?arnumber=00320771

[22] C. A. Barrios. (2009, Jun.). Optical slot-waveguide based biochemical sensors-Review. *Sensors*. [Online]. *9 (6)*, pp. 4751-4765. Available: http://www.mdpi.com/1424-8220/9/6/4751

[23] G. Cocorullo and I. Rendina. (1992, Jan.). Thermo-optical modulation at 1.5 μm in silicon etalon. *Electronics Lett.* [Online]. *28 (1)*, pp. 83-85. Available: http://ieeexplore.ieee.org/xpls/abs_all.jsp?arnumber=255937

[24] T. Toyoda and M. Yabe. (1983, May). The thermal dependence of the refractive indices of fused silica and crystal quartz. *J. Phys. D: Appl. Phys.* [Online]. *16 (5)*, pp. 97-100. Available: http://iopscience.iop.org/0022-3727/16/5/002